

Supplementary Information for

Redox-active pyrene-based pristine porous organic polymers for efficient energy storage with exceptional cyclic stability

Sujoy Bandyopadhyay, Chanderpratap Singh, Priyajit Jash, MD. Waseem Hussain, Amit Paul* and Abhijit Patra*

Department of Chemistry, Indian Institute of Science, Education and Research Bhopal, Bhopal-462066,

E-mail: apaul@iiserb.ac.in, abhijit@iiserb.ac.in

Sr. No.	Contents	Pages
I.	Instrumentation	2-3
II.	Synthesis and characterization	4-9
(i)	Chemicals	4
(ii)	Fabrication of polymers	4-5
(iii)	Characterization of POPs	5-9
III.	Details of morphology and elemental analysis	8-9
(i)	Field Emission Scanning Electron Microscopy (FESEM) and Energy dispersive X-ray (EDX)	8-9
(ii)	Transmission electron microscopy (TEM)	9
IV.	Gas sorption	10
V.	Electrochemical studies	11-21
(i)	Electrode fabrication	11
(ii)	Electrochemical measurements	11-15
(iii)	Discussion related to the cyclic stability of PYBDA	15-17
(iv)	Electrochemical impedance spectroscopy (EIS)	18-21
VI.	A comparative account of supercapacitor performance of PYDA and PYBDA with notable porous solids	22-24
VII.	References	25-26

I. Instrumentation

Fourier transform infrared spectroscopy (FTIR):

FTIR measurements were done on Perkin-Elmer Model 2000 FTIR using KBr pellet. Thirty scans were signal-averaged with a resolution of 8 cm^{-1} at ambient temperature.

Nuclear magnetic resonance (NMR) spectroscopy:

The solid-state ^{13}C -NMR spectra were recorded on a Bruker Avance III 800 MHz (field 18.8 T) standard bore spectrometer equipped with 4 mm solid-state MAS (magic angle spinning) probe. The samples were packed into a 4 mm zirconia rotor and spun at 12.5 kHz at the magic angle. The magic angle was calibrated using ^{79}Br NMR of KBr. The sample temperature was maintained at about 295 K using a Bruker cooling unit with regulated N_2 gas directed at the rotor.

Thermogravimetric analysis (TGA):

TGA analysis was carried out using Perkin Elmer TGA-6000 instrument. The sample was heated at a rate of $10\text{ }^\circ\text{C min}^{-1}$ under a nitrogen atmosphere to a maximum of $700\text{ }^\circ\text{C}$.

Field emission scanning electron microscopy (FESEM):

The surface morphology of all polymers was examined using a Carl Zeiss (Ultraplus) field emission scanning electron microscope. Samples for microscopy were prepared by sprinkling ($\sim 0.5\text{ mg}$) polymers (powdered form) on aluminium stub using an adhesive carbon tape. All samples were coated with a thin layer of sputtered gold prior to imaging. FESEM was carried out using an accelerating voltage of 10 kV and 20 kV.

Energy dispersive X-ray spectroscopy (EDS):

EDS was examined using a spectrometer (Oxford Instruments X-MaxN) attached to FESEM. Measurements were done at a working voltage of 20 kV and elemental Co was used as a reference.

Transmission electron microscopy (TEM):

The morphology of polymers was examined using FEI TALOS 200S instrument at a working voltage of 200 kV. The samples for TEM analysis were prepared by drop casting a homogeneous dilute dispersion of PYDA and PYBDA over a carbon coated 400 mesh Cu grid.

X-ray photo electron spectroscopy (XPS):

The XPS experiment was performed on a sample holder with a vacuum dried powder sample drop of the size 1.5 mm radius using PHI 5000 Versa Prob II, FIE Inc. The scan time was set for one hour per element for core level scan (energy band: 20 eV) with a pass setting of 23.5 eV, 0.025 eV step and 100 ms time per step for 5 cycles.

BET analysis:

All the gas adsorption measurements were performed on a Quantachrome Autosorb, QUANTACHROME QUA211011 equipment. The sample was degassed at 100 °C for 24 h under vacuum before analysis. Isotherms were analyzed using ASiQwin software.

Electrochemical measurements:

All electrochemical experiments were carried using BioLogic SP-300 potentiostat (BioLogic, France). Three electrode electrochemical cell was used for the measurements.

II. Synthesis and characterization

(i) Chemicals: All chemicals were used as received unless stated otherwise. 1,3,6,8-Tetrabromopyrene (97%), 1,4-phenylenediamine (99%), benzidine (98%), bis(dibenzylideneacetone)palladium(0), 2-dicyclohexylphosphino-2',4',6'-triisopropylbiphenyl (XPhos, 97%), potassium *tert*-butoxide (KOtBu, 97%) *N*-methyl-2-pyrrolidone (NMP) and poly(vinylidene fluoride) were purchased from Sigma-Aldrich. Sulfuric acid (H₂SO₄, 99%) was purchased from Sigma-Aldrich. Acetylene black (100%) was purchased from Alfa-Aesar. Platinum foil electrode, platinum (Pt) wire and saturated calomel electrode (SCE) were purchased from CH Instruments Inc. TX, USA.

(ii) Fabrication of polymers

(a) Synthesis of TBDA

1,3,5-Tribromobenzene (1 mmol), benzene-1,4-diamine (2 mmol), bis(dibenzylideneacetone) palladium (0) (15 mol%), 2-dicyclohexylphosphino-2',4',6'-triisopropylbiphenyl (15 mol%), potassium *tert*-butoxide (4 mmol) were taken in a 250 mL Schlenk tube and were dissolved in 50 mL anhydrous toluene. The reaction mixture was stirred at 110 °C for 48 h under nitrogen atmosphere. The reaction mixture was cooled to room temperature and was poured into methanol (200 mL) and the mixture was stirred for 30 minutes. The precipitate was collected by gravimetric filtration and was washed with methanol and acetone. Then the solid polymer was rigorously washed by Soxhlet extraction for 24 h each with methanol, acetone, tetrahydrofuran and chloroform, respectively and was subsequently dried under vacuum at 100 °C for 12 h.

(b) Synthesis of PYDA

1,3,6,8-tetrabromopyrene (1 mmol), 1,4-phenylenediamine (2 mmol), bis(dibenzylideneacetone) palladium (0) (15 mol%), 2-dicyclohexylphosphino-2',4',6'-triisopropylbiphenyl (15 mol%), potassium *tert*-butoxide (4 mmol) were taken in a 250 mL Schlenk tube and were dissolved in 50 mL anhydrous toluene. The reaction mixture was stirred at 110 °C for 48 h under nitrogen atmosphere. The reaction mixture was cooled to room temperature and poured into methanol (200 mL) and was stirred for 30 minutes. The precipitate was collected by gravimetric filtration and washed with methanol and acetone followed by Soxhlet extraction for 24 h each successively with methanol, acetone, tetrahydrofuran and chloroform. The polymer was dried under vacuum at 100 °C for 12 h.

(c) Synthesis of PYBDA

1,3,6,8-Tetrabromopyrene (1 mmol), 4,4'-diaminobiphenyl (2 mmol), bis(dibenzylideneacetone) palladium(0) (15 mol%), 2-dicyclohexylphosphino-2',4',6'-triisopropylbiphenyl (15 mol%), potassium *tert*-butoxide (4 mmol) were taken in a 250 mL Schlenk tube and were dissolved in 50 mL anhydrous toluene. The reaction mixture was stirred at 110 °C for 48 h under nitrogen atmosphere. The reaction mixture was cooled to room temperature and poured into methanol (200 mL) and was stirred for 30 minutes. The precipitate was collected by gravimetric filtration and was washed with methanol and acetone followed by Soxhlet extraction for 24 h each successively with methanol, acetone, tetrahydrofuran and chloroform. The polymer was dried under vacuum at 100 °C for 12 h.

(iii) Characterization of POPs

(a) Fourier transform infrared (FTIR) spectroscopy

The FTIR spectra showed that the primary aryl amine ($-\text{Ph}-\text{NH}_2$) of the linkers converted to secondary amine ($-\text{Ph}-\text{NH}-$) moieties in the CPOPs. The corresponding bending vibrational bands hypsochromically shifted from ~ 1635 to 1596 cm^{-1} and the stretching vibrational bands of C–N of the polymers bathochromically shifted from ~ 1258 to 1290 cm^{-1} (Fig. S1). The C–Br stretching frequency at 1054 cm^{-1} in 1,3,6,8-tetrabromopyrene almost disappeared in CPOPs indicating successful BH coupling between monomer and the corresponding diamines.

(b) Nuclear magnetic resonance (NMR) spectroscopy

The structures of the pristine polymers were analyzed by solid-state ^{13}C -NMR spectroscopy (Fig. S2 and S3). The peak at ~ 144 - 146 ppm owing to the substituted phenyl carbon atoms which connected to the nitrogen atom. The peak at ~ 127 ppm is due to the other aromatic carbons. A low-intensity peak at 158.4 ppm in PYDA is due to the C=N (partial oxidation in air), which is also corroborated with the previous literature.¹

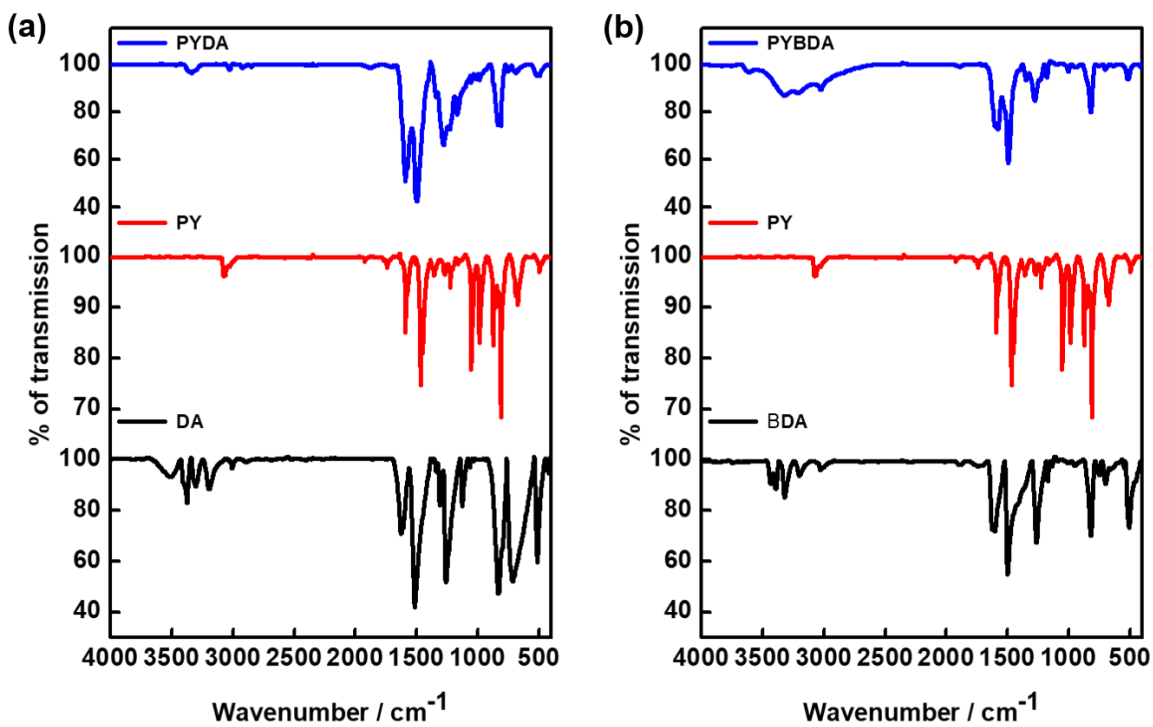


Figure S1 The comparative FTIR spectra of (a) PYDA and (b) PYBDA along with 1,3,6,8-tetrabromopyrene (Py) and the corresponding linkers (DA: 1,4-phenylenediamine and BDA: 4,4'-diaminobiphenyl).

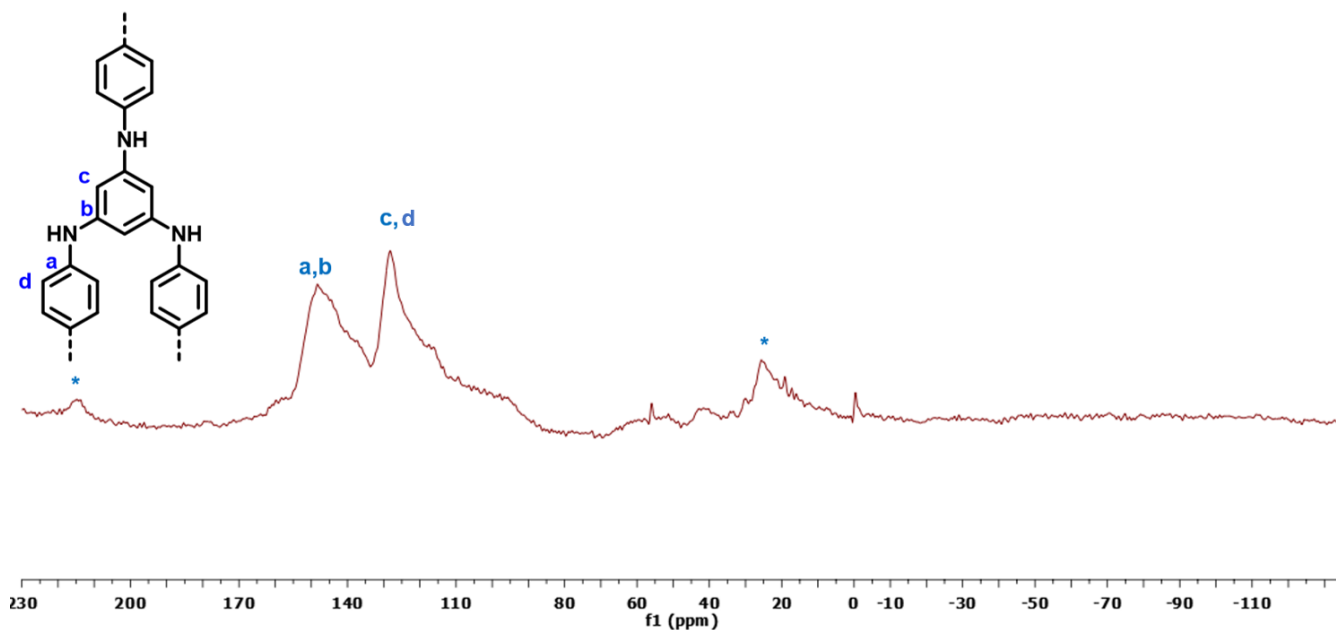


Figure S2 Solid-state ¹³C-NMR spectrum of TBDA.

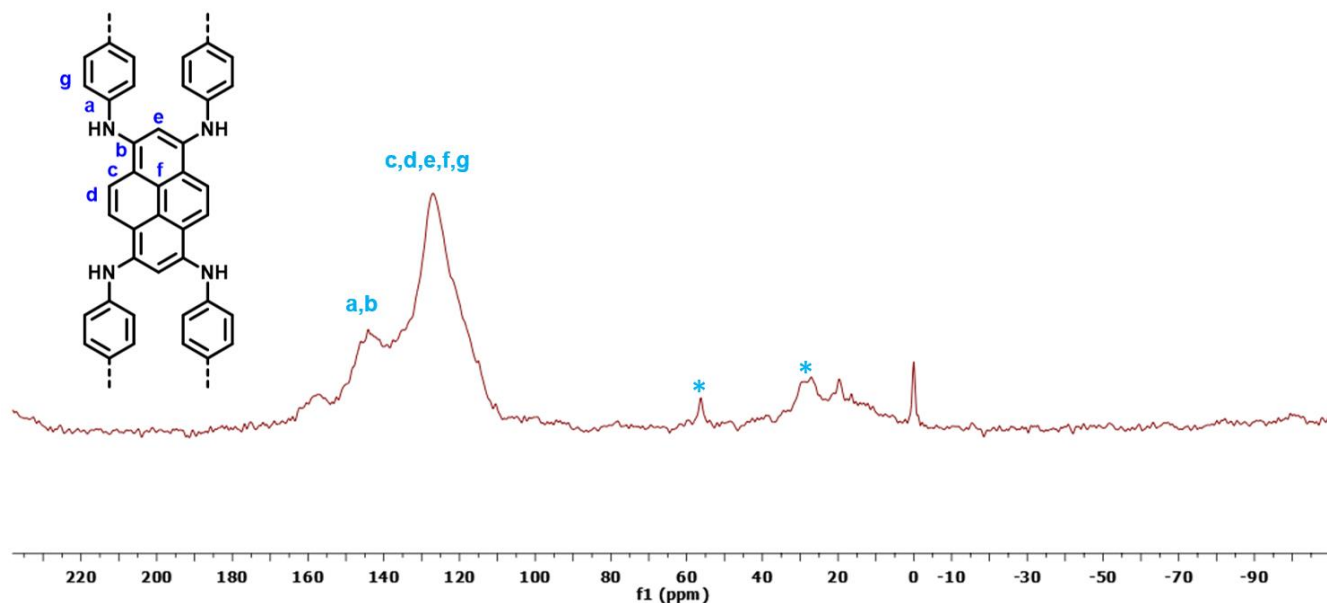


Figure S3 Solid-state ^{13}C -NMR spectrum of PYDA.

(c) Thermogravimetric analysis

Thermogravimetric analysis was carried out through PerkinElmer TGA-6000 instrument by heating the sample at a rate of $10\text{ }^{\circ}\text{C min}^{-1}$ under the nitrogen atmosphere to a maximum of $700\text{ }^{\circ}\text{C}$. Thermogravimetric analysis (TGA) profile of the polymers showed that CPOPs are thermally stable up to $380\text{ }^{\circ}\text{C}$ which indicates the highly cross-linked structure (Fig. S4).

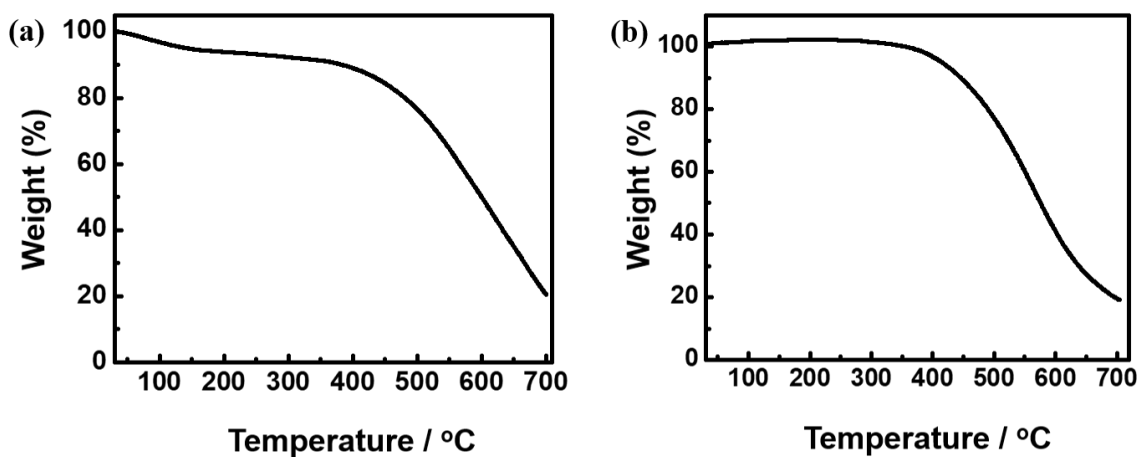


Figure S4 TGA plots of (a) PYDA and (b) PYBDA.

(d) X-ray photoelectron spectroscopy analysis

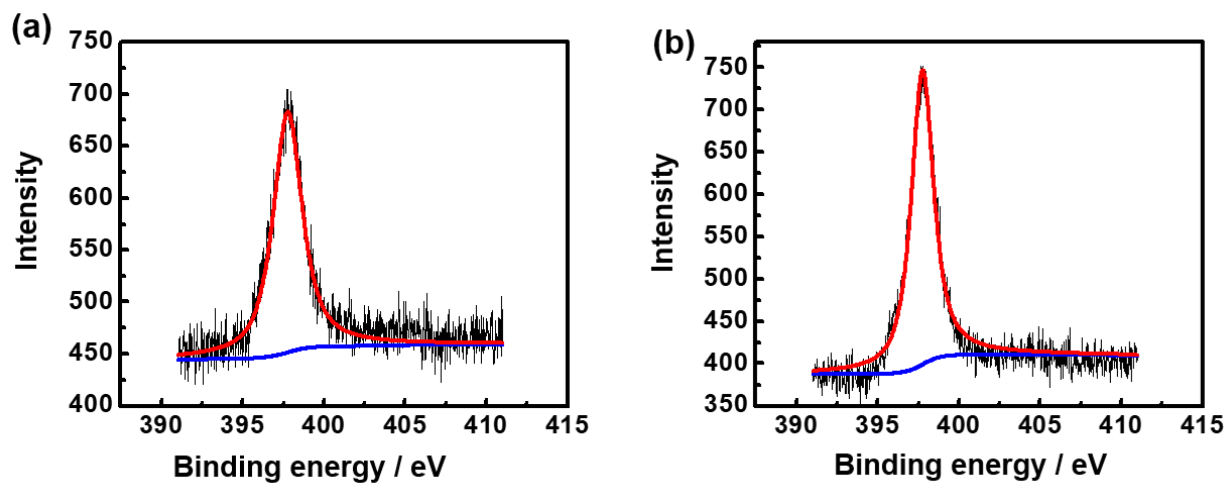


Figure S5 The N 1s XPS spectra of pristine polymers (a) PYDA and (b) PYBDA indicating the peaks at ~ 398 eV.

III. Details of morphology and elemental analysis

(i) Sample preparation for FESEM and EDX analysis: All samples were coated with a thin layer of sputtered gold prior to imaging. FESEM was carried out using an accelerating voltage of 20 kV.

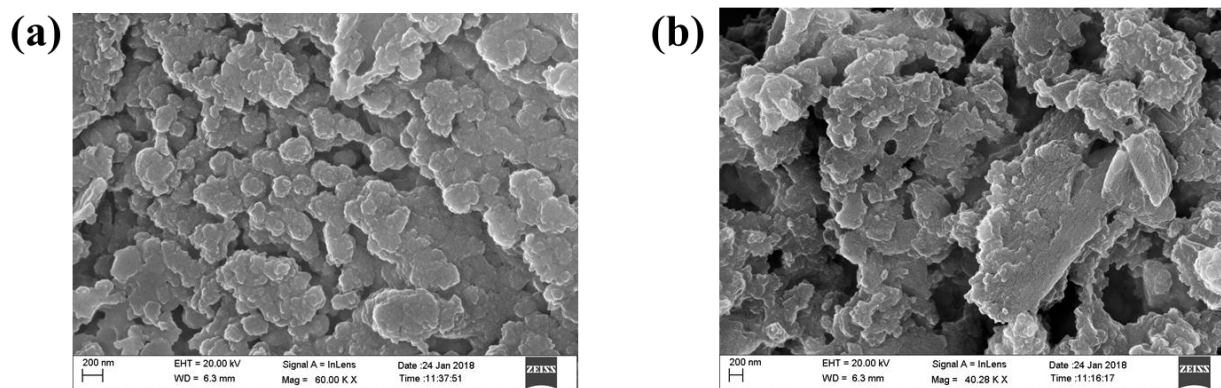


Figure S6 FESEM images of (a) PYDA and (b) PYBDA.

The EDX was performed at a working voltage of 20 kV and was standardized with Co element.

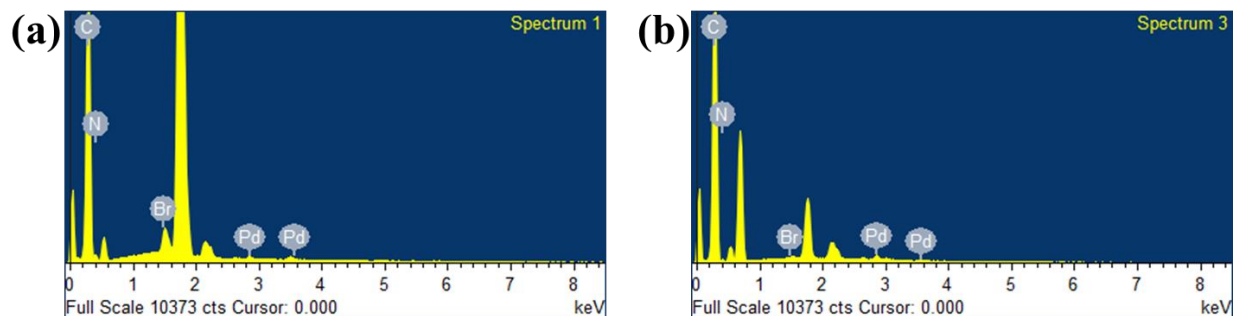


Figure S7 EDX analysis of (a) PYDA (b) PYBDA.

Table S1 Weight and atomic percentages of different elements obtained from EDX analysis.

Polymer	PYDA		PYBDA	
	Weight%	Atomic%	Weight%	Atomic%
C	52.2	59.9	65.2	70.6
N	39.4	38.7	31.1	28.9
Br	7.4	1.3	1.0	0.2
Pd	1.0	0.1	2.6	0.3

(ii) TEM analysis

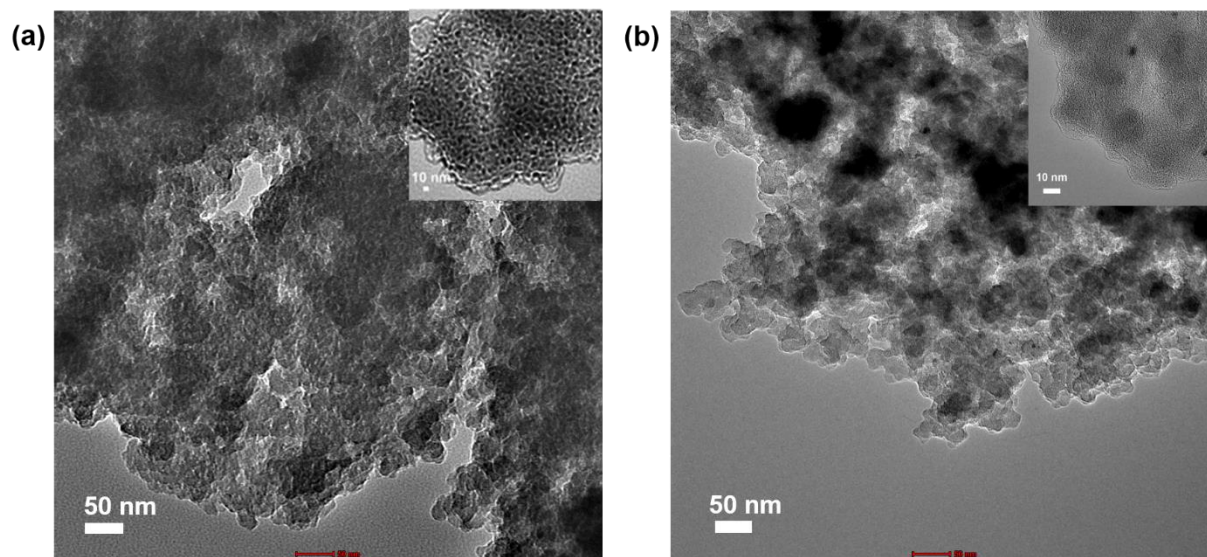


Figure S8 High-resolution TEM images of (a) PYDA and (b) PYBDA, inset: zoom images.

IV. Gas sorption

Details of measurements and sorption isotherms: The samples were degassed at 100 °C for 24 h under vacuum before the analysis. The surface area and pore size distributions of the polymers were measured by nitrogen adsorption-desorption isotherms at 77 K. The pore size distributions were derived from nonlocal density functional theory (NLDFT) method. The details of the specific calculation model are as following: carbon (slit pore, NLDFT equilibrium model).² The high N₂ uptake at the high-pressure region indicates the presence of interparticular void space. The BET surface area of PYDA and PYBDA were found to be 105 m² g⁻¹ and 135 m² g⁻¹, respectively (Fig. S9). The similar increase of surface area of the polymers with increasing the strut length of comonomers fabricated by Buchwald-Hartwig coupling reactions was also observed by Faul and coworkers.¹ The probable reason for increasing the surface area with increasing strut length of the comonomer is the restriction of NH... π interactions leading to a high degree of polymerization. PYDA is mesoporous with the dominant pore size of 2.8 nm. PYBDA is microporous with the pore distribution centered at 1.4 nm. The presence of mesopore was also observed.

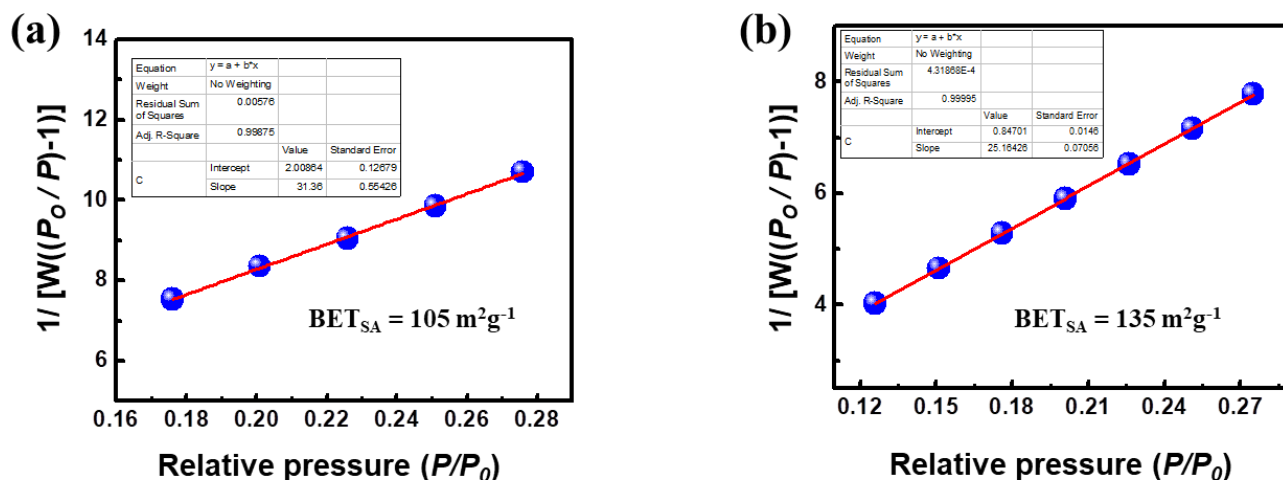


Figure S9 Specific surface area plots of (a) PYDA and (b) PYBDA.

V. Electrochemical studies

(i) Electrode fabrication:

For supercapacitor studies, Pt foils were used as working electrodes and those were coated with CPOPs. First, Pt foils were cleaned in acetone by sonication for half an hour and dried in air. After that, 2 mL *N*-methyl-2-pyrrolidone (NMP), 2 mg acetylene black, 2 mg poly(vinylidene fluoride) (PVDF) binder and 6 mg of CPOPs were added. The mixture was stirred for 8 h to enhance the homogeneity of the dispersion. 100 μ L of the above dispersion was drop casted and spread on Pt foil covering 1 cm² area and dried at 100 °C for 12 h in a hot air oven. The weight ratio of CPOP: acetylene black: PVDF were 3:1:1.

(ii) Electrochemical measurements:

Electrochemical measurements were performed on a BioLogic SP-300 potentiostat (BioLogic, France) using regular three-electrode cell configuration with a saturated calomel electrode (SCE), platinum wire and CPOP coated Pt foil as the reference, counter and working electrodes, respectively. Cyclic voltammetry (CV) experiments were performed at various scan rates in 2 M H₂SO₄ electrolyte solution. Galvanostatic charge/discharge experiments were performed at different current densities in 2 M H₂SO₄ solution as well. Specific capacitances from CVs were obtained using the equation 1. In this equation, C_{sp} , I , ν , m and E denote specific capacitance, current, scan rate, the mass of active material deposited on electrodes and the potential range, respectively. The numerator of this equation was calculated by integrating the area of cyclic voltammograms in Origin software.

$$C_{sp} = \frac{\int I dE}{2 E \nu m} \quad (1)$$

The total specific capacitance has two contributions. The first contribution was due to the double layer formation and the other contribution was due to redox reaction, which is also known as pseudocapacitance. The electrochemical software allows drawing a background line under the redox peaks and provides the charges under the redox peaks. For both anodic and cathodic peaks, the charges were calculated. Summations of charges for two peaks were considered as faradaic charges, which are mathematically equivalent to $(\int I \cdot dE)/\nu$. After that, pseudocapacitance contributions were calculated by dividing the charge by twice of the potential window (E) according to the equation 1. Finally, pseudocapacitances in F/g were calculated by dividing calculated pseudocapacitances by the weight of the material deposited on the electrode. The total specific capacitance is the summation of the double layer and pseudocapacitance

contribution. Hence, by subtracting the pseudocapacitances from the total specific capacitances, the double layer capacitances in F/g were calculated.

Similarly, the specific capacitance from the galvanostatic charge/discharge experiments were calculated utilizing equation 2, wherein t is the time taken for the charge/discharge process.

$$C_{sp} = \frac{I t}{2 E} \quad (2)$$

Electrochemical impedance spectroscopy (EIS) experiments were performed at a potential of 0.15 V vs SCE with an amplitude of 0.01 V over the frequency range of 10^5 to 0.01 Hz.

The energy density and power density were calculated using equation 3 and equation 4, respectively wherein C_{sp} , E , and t are specific capacitance, potential window and discharging time, respectively.

$$\text{Energy density} = \frac{1}{2} C_{sp} \times E^2 \quad (3)$$

$$\text{Power density} = \text{Energy density}/t \quad (4)$$

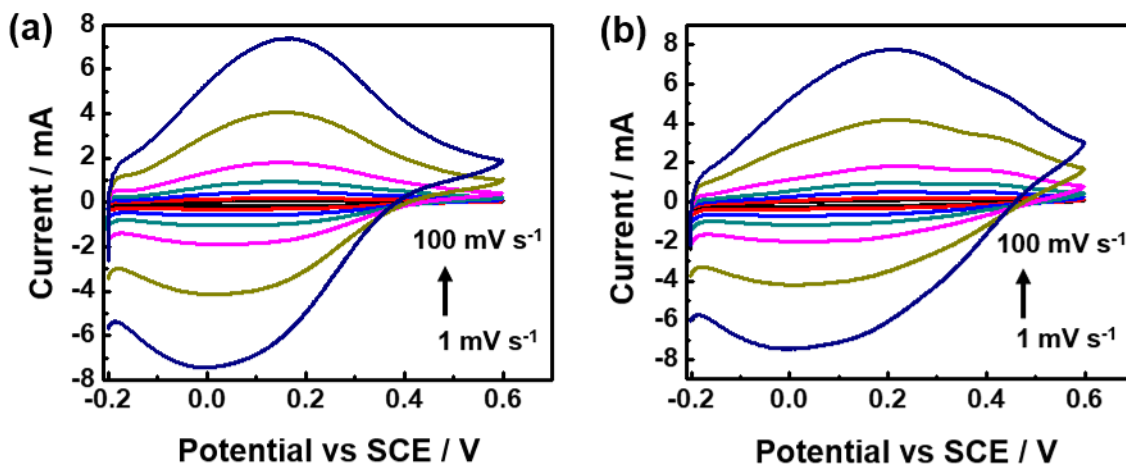


Figure S10 Cyclic voltammograms of (a) PYDA and (b) PYBDA at different scan rate (1-100 mV s⁻¹).

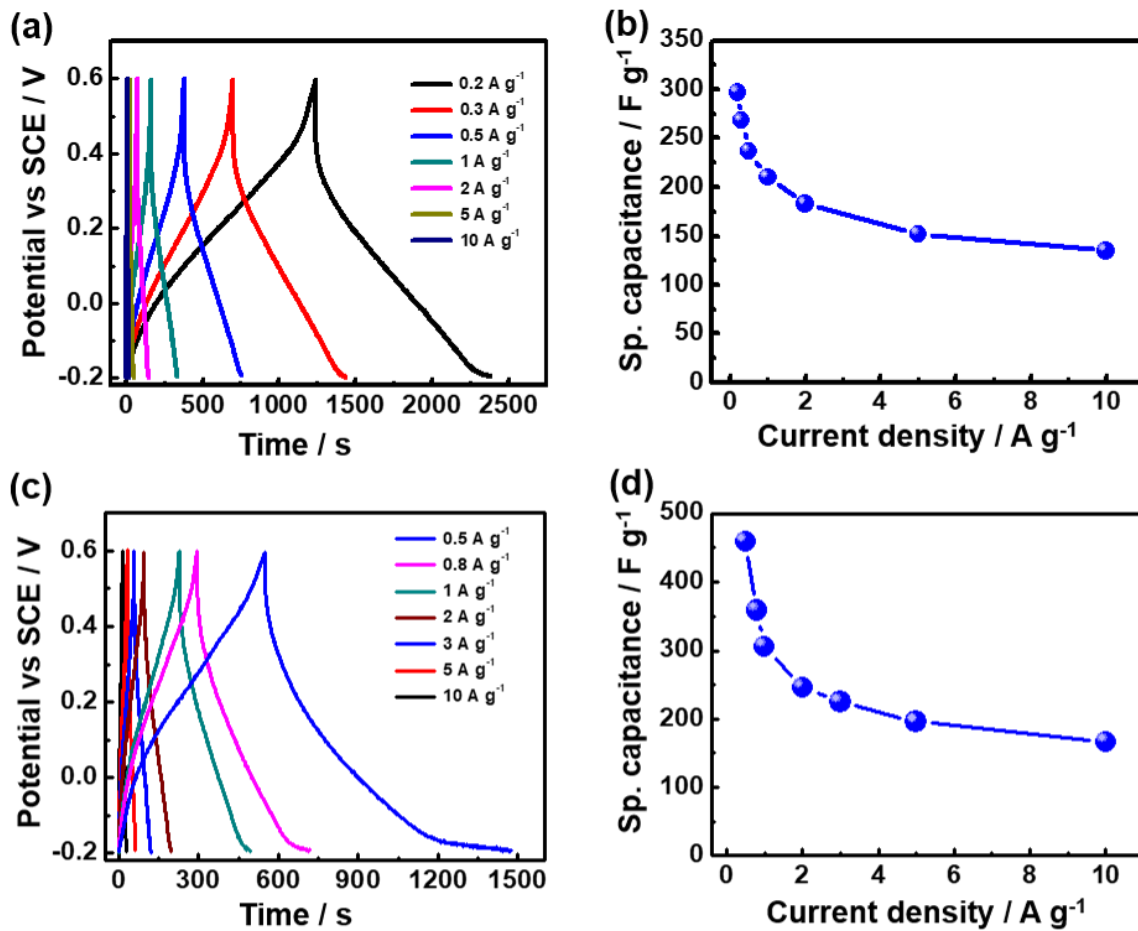


Figure S11 (a) Galvanostatic charge-discharge curves and (b) the corresponding specific capacitances at different current densities of PYDA. (c) The galvanostatic charge-discharge curves and (d) the corresponding specific capacitances at different current densities of PYBDA.

Table S2 Specific capacitances, pseudocapacitance and double layer capacitance calculated from cyclic voltammetry for PYDA and PYBDA obtained at different scan rates (mV s^{-1}) and specific capacitances for PYDA and PYBDA calculated at different current densities (A g^{-1}) from the galvanostatic charge-discharge experiment.

PYDA						PYBDA					
Scan rate (mV s^{-1})	Specific capacitance (F g^{-1})	Double layer capacitance (F g^{-1})	Pseudo capacitance (F g^{-1})	Current density (A g^{-1})	Specific capacitance (F g^{-1})	Scan rate (mV s^{-1})	Specific capacitance (F g^{-1})	Double layer capacitance (F g^{-1})	Pseudo capacitance (F g^{-1})	Current density (A g^{-1})	Specific capacitance (F g^{-1})
100	143	70	73	10	135	100	168	78	90	10	167
50	162	80	82	5	152	50	189	92	97	5	196
20	186	93	93	3	183	20	219	104	115	3	225
10	205	101	104	1	210	10	244	125	119	2	246
5	224	113	111	0.5	237	5	278	151	127	1	306
2	266	136	130	0.3	268	2	332	193	139	0.8	359
1	280	139	141	0.2	297	1	410	260	150	0.5	456
Reten- tion (%)	51.1				45.5		41				36.7

In cyclic voltammetry (CV) experiment, an ideal double-layer capacitor shows rectangular CV curve, wherein faradaic process exhibits peak in CV due to electron transfer across the electrode-electrolyte interface.³ In double layer capacitor, the current instantly raises the maximum value and fast sorption of electrolyte ion occurs. The faradaic reaction where the electron transfer is more sluggish compared to the double layer capacitor. In a double layer capacitor, the high amount of charge can be stored with increasing the surface area of the electrode materials, whereas faradaic capacitance depends upon the redox active functional groups in the materials. We observed the presence of both double layer

capacitance as well as pseudocapacitance in the CV curves of PYDA and PYBDA. The specific capacitance of the polymers was calculated from the cyclic voltammetry curve using the equation 1 and the values at different scan rate are given in the Table S2. Galvanostatic charge-discharge experiments show fast charge-discharge rates. However, the PYDA shows lower discharge time compared to that of PYBDA (Fig. S11). The specific capacitance value was calculated from the basis of discharge time and the specific capacitance value of PYBDA is higher than that of the PYDA providing good agreement with the CV results (Table S2).

(iii) Discussion related to the cyclic stability of PYBDA:

In order to check the long-term cyclic stability of the CPOPs, the cyclic voltammetry experiments at 100 mV s^{-1} scan rate were carried out. The data up to 5000 cycles for PYDA and PYBDA are shown in Fig. 2d, main text. The cyclic stability of PYBDA up to 15000 cycles is shown in Fig. S12. The result demonstrates that with the increasing number of cycles, the specific capacitance value increases as well as a new redox peak appears (Fig. S13). These observations suggest a significant change in the chemical environment of the polymers. We performed the XPS analysis of the electrode materials (PYBDA + PVDF + acetylene black) before and after 5000 cycles. The significant change in the nitrogen environment of PYBDA was observed. The N1s peak at 398.1 eV of pristine polymer decreased and a new peak at 400.2 eV was observed (Fig. S14).⁴

The peak centered at 398.1 eV in N1s XPS spectra (Figure S14) is assignable to the amine nitrogen of PYBDA. After the cyclic test, the contribution of the amine peak is significantly decreased and a new

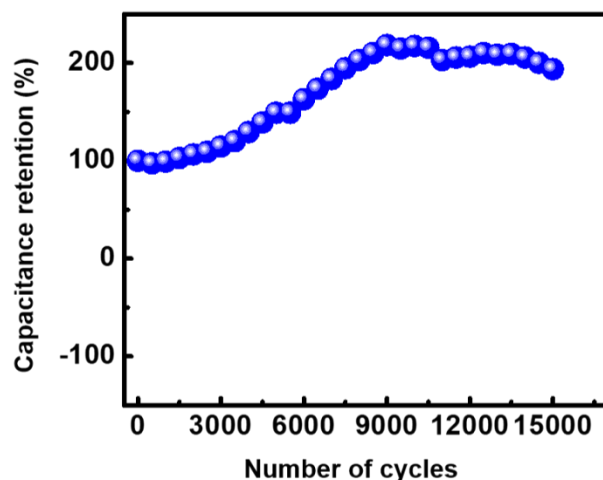


Figure S12 Cyclic stability of PYBDA up to 15000 cycles.

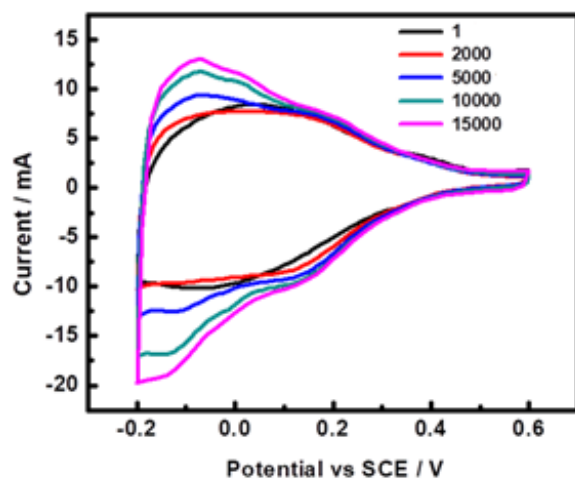


Figure S13 Cyclic voltammograms of PYBDA at 100 mV s⁻¹ scan rate of 1st, 2000, 5000, 10000 and 15000 cycles.

peak at 400.2 eV appears. The high binding energy peak at 400.2 eV can be assigned to the formation of cationic radical nitrogen species.⁴ As proposed by Epstein and coworkers the radical cations are highly

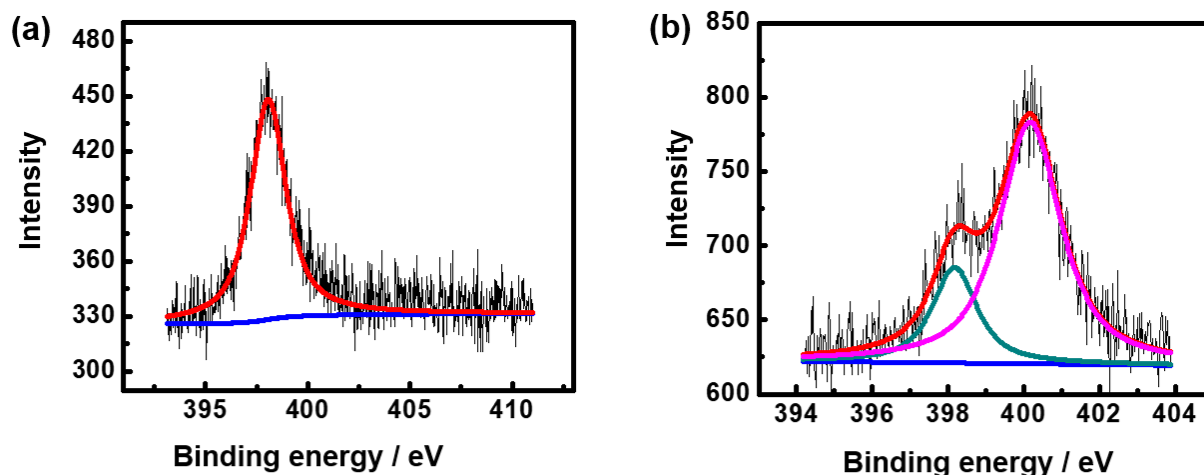


Figure S14 XPS analysis N1s of PYBDA (a) before 5000 cycles and (b) after 5000 cycles.

Table S3 The comparative XPS analysis of N1s of electrode materials involving PYBDA before and 5000 cycles.

	Peak position (eV)	Area	FWHM
Before 5000 cycles	398.1	366.1	2.07
After 5000 cycles	398.2	133.4	1.41
	400.2	464.4	1.94

delocalized and is stabilized by counter anions from the electrolytes (H_2SO_4).⁴ The change in binding energies of C1s of the electrode materials before and after the 5000 cycles is also noticeable (Fig. S15). Further, the cyclic voltammetry measurements at different pH buffers revealed no significant change in the oxidation peak (i.e., no proton removal under the acidic conditions). The plausible redox transformations based on the electrochemical results coupled with the XPS analysis is shown in Fig. S16. The cationic radical nitrogen species are likely to be stabilized in the branched polymeric network assisted by the π -electronic cloud of the polyaromatic ring (pyrene). The efficient delocalization of radical cations throughout the network enhanced the conductivity of the electrode materials leading to the improved supercapacitor performance which was further supported by the electrochemical impedance spectroscopy as discussed below. However, the logical extension of the present communication would be further exploration (e.g., CV coupled with solid-state NMR) along with computational modeling unravelling the detailed molecular level picture.

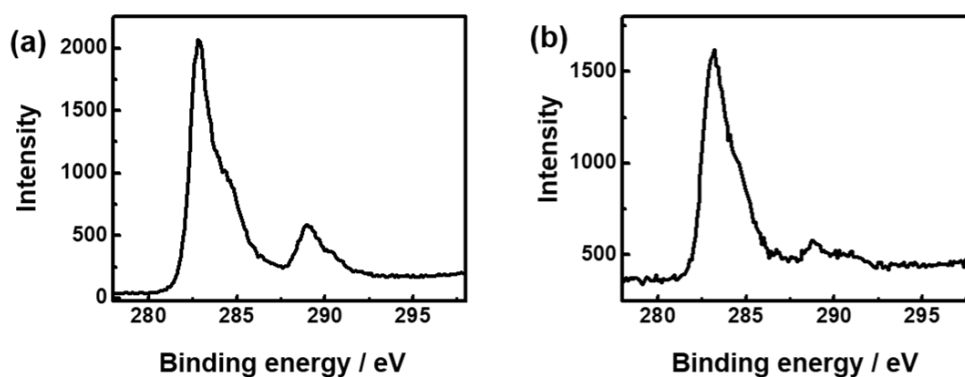


Figure S15 XPS analysis of C1s of the electrode materials involving PYBDA (a) before 5000 cycles (b) after 5000 cycles.

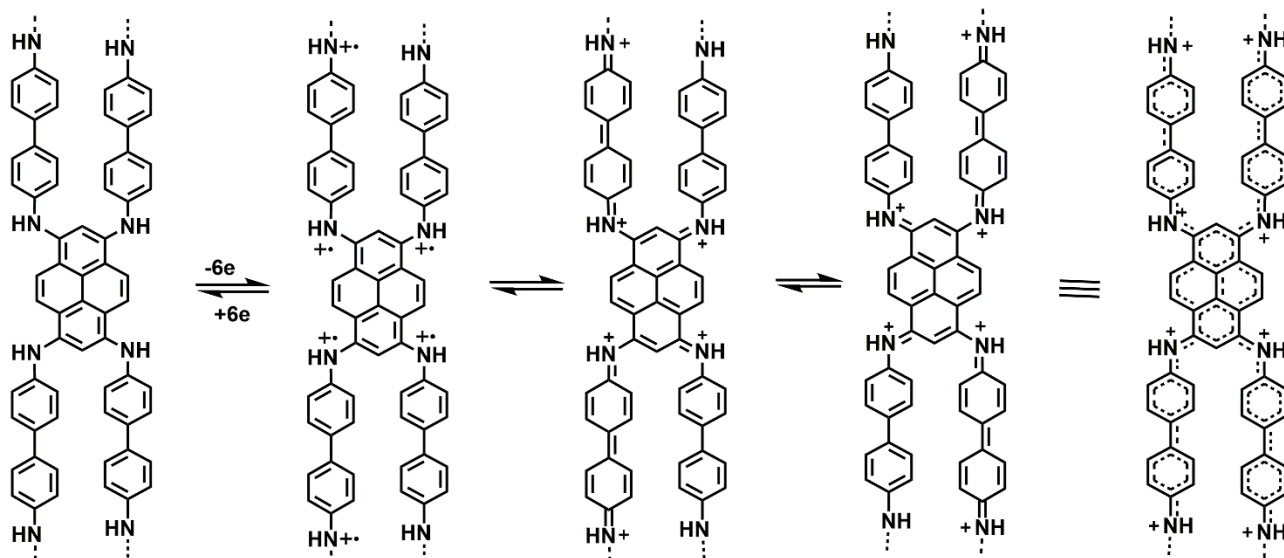


Figure S16 Plausible redox transformations of PYBDA.

(iv) Electrochemical impedance spectroscopy (EIS):

For physical understanding of the charge storage process happened at the electrode/electrolyte interface, electrochemical impedance spectroscopy (EIS) was carried out and the Nyquist plots are shown in Fig. S17. EIS results were fitted according to the equivalent circuits shown in Fig. S17, inset. R_s , R_{ct} , and C_{dl} are solution resistance, charge transfer resistance at the electrode/electrolyte interface and the double layer capacitance at the electrode/electrolyte interface at short time scale. Q_1 , Q_2 and Q_3 are the diffusion capacitance contribution arising through the mass transfer at low frequency region deep inside the material at longer time scale, pseudocapacitive charging, i.e., the passage of electrons inside the porous network and the resistance due to the desorption of ions inside pores, respectively. The fitting of EIS results for PYBDA required an extra circuit element (Q_3) presumably due to desorption of ions at very long timescales.

The complex capacitance ($C(\omega)$) is defined by equation 5. Herein, $C'(\omega)$ and $C''(\omega)$ represent real and imaginary components of complex capacitances and they are further defined by equations 6 and 7, respectively.

$$C(\omega) = C'(\omega) - C''(\omega) \quad (5)$$

$$C'(\omega) = \frac{-Z''(\omega)}{\omega|Z(\omega)|^2} \quad (6)$$

$$C''(\omega) = \frac{-Z'(\omega)}{\omega|Z(\omega)|^2} \quad (7)$$

$C''(\omega)$ vs frequency plot provides a maximum which represents the characteristics frequency (f_0) at which 50% power is delivered and inverse of this frequency is known as dielectric relaxation time constant (τ_0) for whole system or supercapacitor factor of merit (Fig. S19).⁵ EIS data, fitted values and their time constants values for different systems were tabulated in Table S4. Q_1 , Q_2 and Q_3 are constant phase elements defined by the following equation.

$$Z_{CPE} = \frac{1}{(j\omega)^a Q} \quad (8)$$

Z_{CPE} is the total impedance due to a particular constant phase element (Q). The constant phase elements are frequency (ω) dependent and the exponent term ' a ' can range from 0 to 1 while '0' and '1' represent an ideal resistor and an ideal capacitor behavior, respectively. It is important to note that, electrochemical behavior deviates significantly from ideal resistor and capacitor and hence values are obtained in between 0 and 1. Q_2 represents pseudocapacitive charging, i.e., passage of electrons inside the nanomaterial.

EIS analysis for PYBDA was performed at the beginning of the cyclic test and at 2000, 5000 and 15000th cycles as well in order to understand the specific capacitance enhancement beyond 2000 cycles. Table S2 suggest that as the cyclic test progressed, charge transfer resistance (R_{ct}) at the electrode-electrolyte interface decreased significantly while double layer capacitance at the electrode-electrolyte interface (C_{dl}) at short time scale increased substantially, suggesting decrease of surface roughness of the electrode-electrolyte interface which helped to improve electron conductivity and double layer formation during cyclic test. However, a closer look at the Table S4 also revealed that the mass transport parameter (Q_1, a_1) started to show noticeable improvement only beyond 2000 cycle. It is important to emphasize that unless mass transport inside the nanomaterials improves, the specific capacitance cannot increase significantly and hence the cyclic test demonstrated significant specific capacitance improvement beyond 2000 cycles. As a consequence, pseudocapacitive charging (Q_2, a_2) also improved significantly beyond 2000 cycles.⁶

Table S4. The values of equivalent circuit parameters calculated from EIS results for PYDA, PYBDA and PYBDA after 2000, 5000 and 15000 cycles at 0.15 V vs. SCE.

Parameters	PYDA	PYBDA	PYBDA after 2000 cycles	PYBDA after 5000 cycles	PYBDA after 15000 cycles
R_s (Ω)	0.50	0.50	0.33	0.45	0.52
C_{dl} (mF)	0.178	0.265	3.20	3.49	11.1
R_{ct} (Ω)	0.90	0.50	0.30	0.15	0.20
Q_1 ($F s^{(a_1-1)}$)	0.34	0.38	0.50	0.45	0.87
a_1	0.22	0.30	0.30	0.40	0.56
Q_2 ($F s^{(a_2-1)}$)	0.04	0.04	0.05	0.06	0.08
a_2	0.85	0.91	0.91	0.91	0.95
Q_3 ($F s^{(a_3-1)}$)		0.0021	0.0020	0.0027	0.0036
a_3		0.35	0.40	0.12	0.026
χ^2	0.0250	0.0187	0.388	0.082	0.093
τ_0 (s)	3.9	0.57	0.82	0.89	0.61

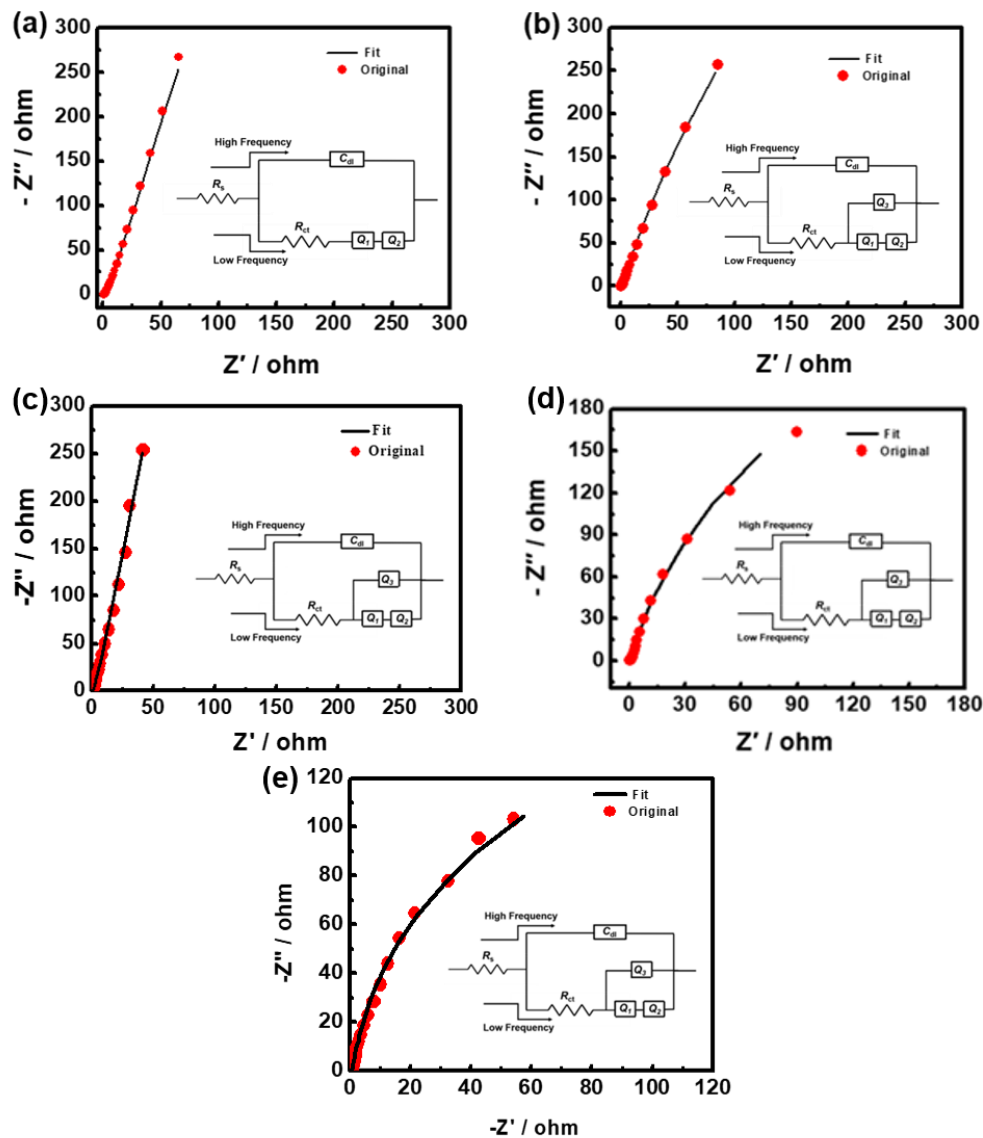


Figure S17 Nyquist plots of (a) PYDA (b) PYBDA (c) PYBDA after 2000 cycles (d) PYBDA after 5000 cycles and (e) PYBDA after 15000 cycles measured at 0.15 V vs SCE in 2 M H_2SO_4 ; inset: the corresponding equivalent circuits.

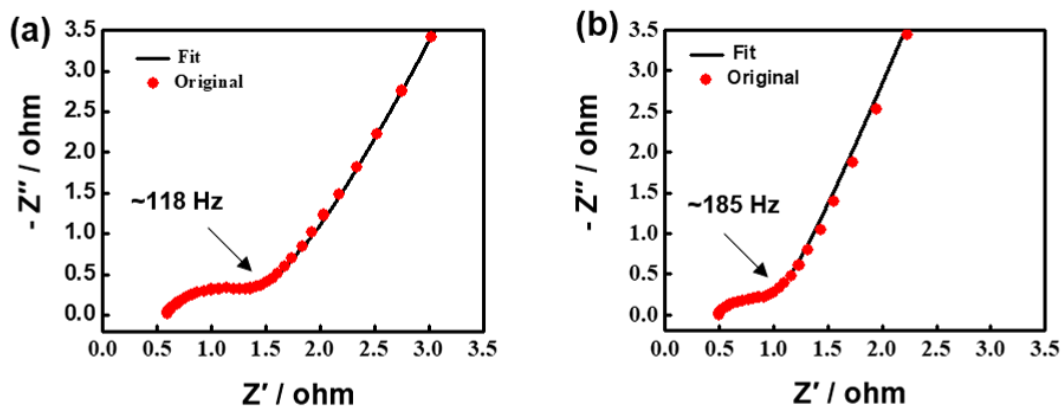


Figure S18 High-frequency region of Nyquist plots of (a) PYDA and (b) PYBDA.

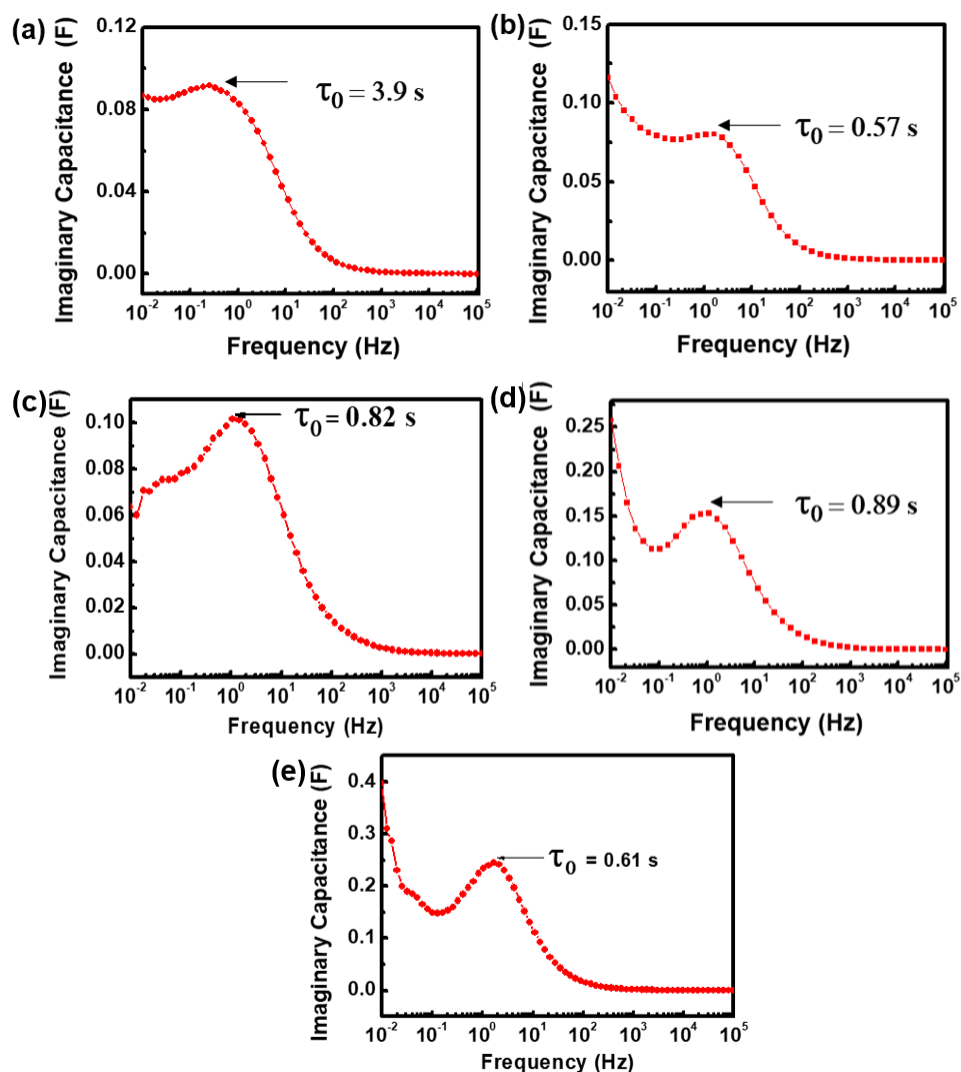


Figure S19 Imaginary capacitance vs frequency for (a) PYDA, (b) PYBDA (c) PYBDA after 2000 cycles (d) PYBDA after 5000 cycles and (e) PYBDA after 15000 cycles.

Table S5 The percentage of yield and specific capacitance of PYDA and PYBDA obtained from different batches of synthesis.

POPs	Batches	Percentage of yield	Average yields	Specific capacitance @ 1 mV s ⁻¹
PYDA	Batch -1	87 %	89 %	280 F g ⁻¹
	Batch -2	92 %		271 F g ⁻¹
	Batch -3	88 %		273 F g ⁻¹
PYBDA	Batch -1	82 %	80 %	410 F g ⁻¹
	Batch -2	78 %		406 F g ⁻¹

VI. A comparative account of supercapacitor performance of PYDA and PYBDA with notable porous solids

Table S6 Comparison of specific capacitance of PYDA and PYBDA with some of the best known porous materials derived from porous organic polymers (POPs), covalent polymer frameworks (CPFs), conjugated microporous polymers (CMPs) and porous carbon based on them ($> 100 \text{ F g}^{-1}$ at 0.2 A g^{-1} or higher current density).

S. No	Electrode materials	Electrolyte	Specific capacitance (F g^{-1})	Cyclic stability	Reference
1	PYDA based POPs	2 M H_2SO_4	297 @ 0.2 A g^{-1}	5000	This work
2	PYBDA based POPs	2 M H_2SO_4	456 @ 0.5 A g^{-1}	15,000	This work
3	PAQTA (Pristine POP)	0.5 M H_2SO_4	576 @ 1 A g^{-1}	6,000	<i>Adv. Mater.</i> , 2018, 30 , 1705710. ⁷
4	TpDAB based (Pristine CPF)	Aq. Na_2SO_4	432 @ 0.5 A g^{-1}	1000	<i>Chem. Commun.</i> , 2016, 52 , 7592. ⁸
5	TPDA-1 (Pristine POP)	1 M H_2SO_4	348 @ 0.5 A g^{-1}	1000	<i>ACS Sustain. Chem. Eng.</i> 2018, 6 , 202. ⁹
6	TAT-CMP-2 (Pristine POP)	1 M Na_2SO_4	183 @ 1 A g^{-1}	10,000	<i>Chem. Sci.</i> , 2017, 8 , 2959. ¹⁰
7	PTCT-C CMP based porous carbon	6 M KOH	558 @ 1 A g^{-1}	1,000	<i>Chem. Mater.</i> , 2017, 29 , 4885. ¹¹
8	N-doped carbon from microporous organic networks	H_2SO_4	286 @ 1 A g^{-1}	10,000	<i>ACS Sustain. Chem. Eng.</i> , 2018, 6 , 3525. ¹²
9	CMP-based hollow, spherical nitrogen-rich porous carbon	5 M KOH	230 @ 0.5 A g^{-1}	1500	<i>ACS Appl. Mater. Interfaces</i> , 2013, 5 , 10280. ¹³

Table S7 Comparison of supercapacitor energy storage of PYDA and PYBDA with some of the notable porous materials including porous carbon, covalent organic frameworks (COFs) and metal oxide nanomaterials ($> 100 \text{ F g}^{-1}$ at 0.2 A g^{-1} or higher current density).

S. No	Electrode materials	Electrolyte	Specific capacitance (F g^{-1})	Cyclic stability	Reference
1	PYDA based POPs	2 M H_2SO_4	297 @ 0.2 A g^{-1}	5000	This work
2	PYBDA based POPs	2 M H_2SO_4	456 @ 0.5 A g^{-1}	15,000	This work
3	HLPC 3D honeycomb-like porous carbon QNPC12-700	6 M KOH	342 @ 0.2 A g^{-1}	1,000	<i>Nanoscale</i> , 2014, 6 , 13831. ¹⁴
4	2D quasi-ordered nitrogen enriched porous carbon GMP2NC	6 M KOH	426 @ 1 A g^{-1}	10,000	<i>Nanoscale</i> , 2016, 8 , 10166. ¹⁵
5	Graphene-based porous carbon PNHCS	6 M KOH	273 @ 0.2 A g^{-1}	5,000	<i>Mater. Chem. Front.</i> , 2017, 1 , 278. ¹⁶
6	Porous nitrogen-doped hollow carbon spheres CDMMC	6 M KOH	213 @ 0.5 A g^{-1}	5,000	<i>J. Mater. Chem. A</i> , 2014, 2 , 5352. ¹⁷
7	Hierarchical cashmere derived micro-/mesoporous carbon	1 M H_2SO_4 6 M KOH	460 @ 0.5 A g^{-1} 363 @ 0.5 A g^{-1}	5,000	<i>Green Chem.</i> , 2015, 17 , 2373. ¹⁸
8	TpPa-(OH) ₂ (pristine COF)	1 M Phosphate Buffer	416 @ 0.5 A g^{-1}	10,000	<i>Chem. Mater.</i> , 2017, 29 , 2074. ¹⁹
9	TDFP-1 (Pristine COF)	0.1 M H_2SO_4	418 @ 0.5 A g^{-1}	1000	<i>ChemSusChem</i> , 2017, 10 , 921. ²⁰
10	TaPa-Py COF	1 M H_2SO_4	209 @ 0.5 A g^{-1}	6,000	<i>J. Mater. Chem. A</i> , 2016, 4 , 16312. ²¹

11	TAPT-DHTA-COF _{0.1} based porous carbon	6 M KOH	411 @ 0.5 A g ⁻¹	10,000	<i>Chem. Commun.</i> , 2017, 53 , 11690. ²²
12	oxygen functionalized few-layer graphene	2 M H ₂ SO ₄	296 @ 0.5 A g ⁻¹	2000	<i>Chem. Commun.</i> , 2016, 52 , 12661. ²³
13	Reduced graphene	2 M H ₂ SO ₄	163 @ 1 A g ⁻¹	1000	<i>J. Mater. Chem. A</i> , 2015, 3 , 18557. ²⁴
14	(COF-LZU1)/ Fe ₃ O ₄ Composite	0.5 (M) H ₂ SO ₄	112 @ 0.5 A g ⁻¹	2,000	<i>ACS Macro Lett.</i> , 2017, 6 , 1444. ²⁵
15	MnO ₂ -KBs nanoparticles	1 (M) Na ₂ SO ₄	272 @ 0.5 A g ⁻¹	5,000	<i>Chem. Eur. J.</i> , 2017, 23 , 4216. ²⁶
16	Fe ₃ O ₄ nanoparticles	1 (M) Na ₂ SO ₃	207 @ 0.4 A g ⁻¹	2,000	<i>Nanoscale</i> , 2013, 5 , 3793. ²⁷

VII. References

1. (a) Y. Liao, J. Weber and C. F. J. Faul, *Chem. Commun.*, 2014, **50**, 8002; (b) Y. Liao, J. Weber, B. M. Mills, Z. Ren and C. F. J. Faul, *Macromolecules*, 2016, **49**, 6322.
2. M. Thommes, K. Kaneko, A. V. Neimark, J. P. Olivier, F. Rodriguez-Reinoso, J. Rouquerol and K. S. W. Sing, *Pure Appl. Chem.*, 2015, **87**, 1051.
3. G. Wang, L. Zhang and J. Zhang, *Chem. Soc. Rev.*, 2012, **41**, 797.
4. J. Yue and A. J. Epstein, *Macromolecules*, 1991, **24**, 4441.
5. A. M and A. Paul, *ACS Omega*, 2017, **2**, 8039.
6. *Electrochemical Methods: Fundamentals and Applications*, A. J. Bard and L. R. Faulkner, Wiley, New York, 1980.
7. Y. Liao, H. Wang, M. Zhu and A. Thomas, *Adv. Mater.*, 2018, **30**, 1705710.
8. B. C. Patra, S. Khilari, L. Satyanarayana, D. Pradhan and A. Bhaumik, *Chem. Commun.*, 2016, **52**, 7592.
9. P. Bhanja, S. K. Das, K. Bhunia, D. Pradhan, T. Hayashi, Y. Hijikata, S. Irle and A. Bhaumik, *ACS Sustain. Chem. Eng.*, 2018, **6**, 202.
10. X. Li, Y. Zhang, C. Wang, Y. Wan, W. Lai, H. Pang and W. Huang, *Chem. Sci.*, 2017, **8**, 2959.
11. H. Wang, Z. Cheng, Y. Liao, J. Li, J. Weber, A. Thomas and C. F. J. Faul, *Chem. Mater.*, 2017, **29**, 4885.
12. J. Lee, J. Choi, D. Kang, Y. Myung, S. M. Lee, H. J. Kim, Y. Ko, S. Kim and S. U. Son, *ACS Sustain. Chem. Eng.*, 2018, **6**, 3525.
13. X. Liu, L. Zhou, Y. Zhao, L. Bian, X. Feng and Q. Pu, *ACS Appl. Mater. Interfaces*, 2013, **5**, 10280.
14. Q. Liang, L. Ye, Z. Huang, Q. Xu, Y. Bai, F. Kang and Q. Yang, *Nanoscale*, 2014, **6**, 13831.
15. K. Kan, L. Wang, P. Yu, B. Jiang, K. Shi and H. Fu, *Nanoscale*, 2016, **8**, 10166.
16. K. Yuan, T. Hu, Y. Xu, R. Graf, L. Shi, M. Forster, T. Pichler, T. Riedl, Y. Chen and U. Scherf, *Mater. Chem. Front.*, 2017, **1**, 278.
17. J. Han, G. Xu, B. Ding, J. Pan, H. Dou and D. R. MacFarlane, *J. Mater. Chem. A*, 2014, **2**, 5352.
18. L. Zhou, H. Cao, S. Zhu, L. Hou and C. Yuan, *Green Chem.*, 2015, **17**, 2373.
19. S. Chandra, D. R. Chowdhury, M. Addicoat, T. Heine, A. Paul and R. Banerjee, *Chem. Mater.*, 2017, **29**, 2074.

20. P. Bhanja, K. Bhunia, S. K. Das, D. Pradhan, R. Kimura, Y. Hijikata, S. Irle, and A. Bhaumik, *ChemSusChem.*, 2017, **10**, 921.
21. A. M. Khattak, Z. A. Ghazi, B. Liang, N. A. Khan, A. Iqbal, L. Li and Z. Tang, *J. Mater. Chem. A*, 2016, **4**, 16312.
22. Q. Xu, Y. Tang, L. Zhai, Q. Chen and D. Jiang, *Chem. Commun.*, 2017, **53**, 11690.
23. C. Singh, N. S., A. Jana, A. K. Mishra and A. Paul, *Chem. Commun.*, 2016, **52**, 12661.
24. C. Singh, A. K. Mishra and A. Paul, *J. Mater. Chem. A*, 2015, **3**, 18557.
25. Y. Liao, J. Li, and A. Thomas, *ACS Macro Lett.*, 2017, **6**, 1444.
26. Q. Maqbool, C. Singh, P. Jash, A. Paul and A. Srivastava, *Chem. Eur. J.*, 2017, **23**, 4216.
27. L. Wang, H. Ji, S. Wang, L. Kong, X. Jiang and G. Yang, *Nanoscale*, 2013, **5**, 3793.